

UNIVERSITY OF BIRMINGHAM

Research at Birmingham

Enhancing thermal performance of a two-phase closed thermosyphon with an internal surface roughness

Alammar, Ahmed A.; Al-mousawi, Fadhel N.; Al-dadah, Raya K.; Mahmoud, Saad M.; Hood, Richard

DOI:

[10.1016/j.jclepro.2018.03.020](https://doi.org/10.1016/j.jclepro.2018.03.020)

License:

Creative Commons: Attribution-NonCommercial-NoDerivs (CC BY-NC-ND)

Document Version

Peer reviewed version

Citation for published version (Harvard):

Alammar, AA, Al-mousawi, FN, Al-dadah, RK, Mahmoud, SM & Hood, R 2018, 'Enhancing thermal performance of a two-phase closed thermosyphon with an internal surface roughness' *Journal of Cleaner Production*, vol. 185, pp. 128-136. <https://doi.org/10.1016/j.jclepro.2018.03.020>

[Link to publication on Research at Birmingham portal](#)

Publisher Rights Statement:

Published in *Journal of Cleaner Production* on 03/03/2018

DOI: 10.1016/j.jclepro.2018.03.020

General rights

Unless a licence is specified above, all rights (including copyright and moral rights) in this document are retained by the authors and/or the copyright holders. The express permission of the copyright holder must be obtained for any use of this material other than for purposes permitted by law.

- Users may freely distribute the URL that is used to identify this publication.
- Users may download and/or print one copy of the publication from the University of Birmingham research portal for the purpose of private study or non-commercial research.
- User may use extracts from the document in line with the concept of 'fair dealing' under the Copyright, Designs and Patents Act 1988 (?)
- Users may not further distribute the material nor use it for the purposes of commercial gain.

Where a licence is displayed above, please note the terms and conditions of the licence govern your use of this document.

When citing, please reference the published version.

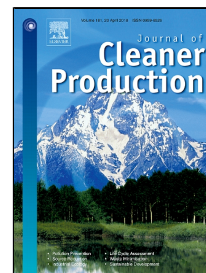
Take down policy

While the University of Birmingham exercises care and attention in making items available there are rare occasions when an item has been uploaded in error or has been deemed to be commercially or otherwise sensitive.

If you believe that this is the case for this document, please contact UBIRA@lists.bham.ac.uk providing details and we will remove access to the work immediately and investigate.

Accepted Manuscript

Enhancing Thermal performance of a Two-phase Closed Thermosyphon With an Internal Surface Roughness

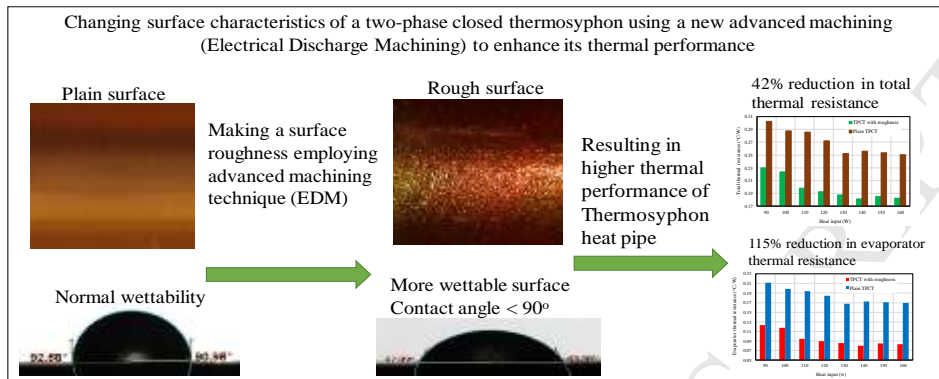


Ahmed A. Alammam, Fadhel N. Al-Mousawi, Raya K. Al-Dadah, Saad M. Mahmoud, Richard Hood

PII: S0959-6526(18)30671-1
DOI: 10.1016/j.jclepro.2018.03.020
Reference: JCLP 12278
To appear in: *Journal of Cleaner Production*
Received Date: 06 January 2018
Revised Date: 20 February 2018
Accepted Date: 02 March 2018

Please cite this article as: Ahmed A. Alammam, Fadhel N. Al-Mousawi, Raya K. Al-Dadah, Saad M. Mahmoud, Richard Hood, Enhancing Thermal performance of a Two-phase Closed Thermosyphon With an Internal Surface Roughness, *Journal of Cleaner Production* (2018), doi: 10.1016/j.jclepro.2018.03.020

This is a PDF file of an unedited manuscript that has been accepted for publication. As a service to our customers we are providing this early version of the manuscript. The manuscript will undergo copyediting, typesetting, and review of the resulting proof before it is published in its final form. Please note that during the production process errors may be discovered which could affect the content, and all legal disclaimers that apply to the journal pertain.



Enhancing Thermal performance of a Two-phase Closed Thermosyphon With an Internal Surface Roughness

Ahmed A. Alammari^{a,b}, Fadhel N. Al-Mousawi^a, Raya K. Al-Dadah^a, Saad M. Mahmoud^a, Richard Hood^a

^a Department of Mechanical Engineering, University of Birmingham
Edgbaston, Birmingham, B15 2TT, Ghulfus_eng@yahoo.com

^b Training and Development Office, Ministry of Electricity, Baghdad, Iraq

Abstract

Enhancement of energy conversion devices has become an important task to reduce size and cost, and design efficient systems. In this work, enhancement of heat transfer performance of a two-phase closed thermosyphon has been investigated by making an internal surface roughness. Thus, a new advanced machining technique (Electrical Discharge Machining) is employed to modify the surface characteristics of a TPCT. The experimental work has been carried out at two initial sub-atmospheric pressures (3 and 30 kPa), heat input range of (90-160 W) and a fill ratio of 50% using water as a working fluid. The results of the new thermosyphon have been compared with a plain copper TPCT to consider the enhancement in thermal performance resulting from resurfacing of the thermosyphon wall. The results revealed that using internal wall roughness in TPCT can enhance its thermal performance by reducing the evaporator temperature, thereby the total thermal resistance decreasing by about 42% and 13% at initial pressures of 3 kPa and 30 kPa, respectively. On the other hand, the evaporator thermal resistance decreases and the evaporator heat transfer coefficient increases by about 115% and 68% at initial pressures of 3 kPa and 30 kPa, respectively. However, the condenser thermal performance decreases using the resurfaced TPCT compared with plain thermosyphon.

Keywords: Two-phase closed thermosyphon; Surface roughness; Thermal performance enhancement; Thermal resistance.

NOMENCLATURE

D	Diameter of thermosyphon	m	Subscripts	
h	Heat transfer coefficient	W/m ² °C	av	Average
I	Current	Am	c	Condenser
K	Thermal conductivity	W/m °C	e	Evaporator
Q	heat input	W	i	Inside
R	Thermal resistance	°C/W	o	Outside
T	Temperature	°C	t	total
V	Voltage	v		

29 **1.Introduction**

30 Energy demand has increased rapidly worldwide due to inefficient use and conversion of energy in
31 different applications. Therefore, reduction of losses and enhancing heat transfer processes in energy
32 systems have become an essential area of research in recent years (Jouhara et al. 2017). Heat pipe offer
33 an effective way to transfer thermal energy by utilising the latent heat of the working fluid by means of
34 evaporation and condensation passively in a closed container. Due to their relatively low thermal
35 resistance, compact and employing a small quantity of the working fluid, they have widely used in
36 different applications such as solar thermal systems, heat exchangers and electronics cooling. Heat
37 pipes consist of two main sections: the evaporator where the heat is absorbed by the working
38 fluid; and the condenser in which heat is rejected. After the heat is added to the evaporator
39 section, the liquid reaches its saturation temperature and evaporates generating vapour. Due to
40 the difference in the vapour pressure between the evaporator and the condenser, it rises to the
41 condenser (with the assistance of the bouncy forces) where it condenses delivering its latent
42 heat to the coolant at the condenser. At that time, the vapour condenses due to a lower
43 temperature in the condenser and returns to the evaporator by gravity, if the heat pipe is
44 wickless (thermosiphon), or by capillary force, if a wick heat pipe is used. A special attention
45 has been paid to a two-phase closed thermosyphon (TPCT) due to its simplicity and cost-effectiveness
46 (Alammar et al. 2017).

47 Electrical Discharge Machining (EDM) is an advanced fully controlled technique that uses the electric
48 spark to remove small pieces from a metal workpiece forming different shapes or surface roughness.

49 This performs by applying a high-frequency electrical current through an electrode which producing a
50 very high-temperature resulting in erosion of a tiny piece of the metal. The electrode is controlled to
51 erode a specified thickness of metal from the sample. Both the workpiece and electrode are submerged
52 in a dielectric fluid for cooling purposes and removing the resulting eroded material (Johnson Waukesha
53).

54 Several research works have been carried out to investigate enhancing the thermal performance of heat
55 pipes using two different techniques. The first technique employs addition of nanoparticles to the
56 working fluid to increase its thermal conductivity and enhance heat pipe performance. Different studies
57 have investigated the effect of using various nanoparticles with water such as CuO nanoparticles (Yang
58 et al. 2008; Liu et al. 2010; Manimaran et al. 2012; Cheedarala et al. 2016), Al₂O₃ nanoparticles (Noie
59 et al. 2009; Aly et al. 2017), silver nanoparticles (Paramatthanuwat et al. 2010; Ghanbarpour et al.
60 2015), iron oxide nanoparticles (Huminic et al. 2011; Huminic & Huminic 2013), graphene
61 nanoparticles (Sadeghinezhad et al. 2016) and multiwalled carbon nanotubes functionalized with ethyl-
62 enediamine EDA-MWCNT nanoparticles (Shanbedi et al. 2012a). It was found that the best
63 nanoparticles concentration which provided the highest thermal performance was 1.0wt%
64 (Yang et al. 2008; Shanbedi et al. 2012b), 0.1wt% (Sadeghinezhad et al. 2016), 0.06wt%
65 (Cheedarala et al. 2016) and 3wt% (Aly et al. 2017). Different studies showed that using
66 nanofluid increased the heat transfer coefficient by 46% (Yang et al. 2008) and 30.4% (Aly et
67 al. 2017), increased CHF by 30% (Yang et al. 2008) and 79% (Cheedarala et al. 2016),
68 increased thermal performance (Liu et al. 2010), by 14.7% (Noie et al. 2009), 70%
69 (Paramatthanuwat et al. 2010), 93% (Shanbedi et al. 2012b), 37.2% (Sadeghinezhad et al.
70 2016) and reduced the thermal resistance (Sureshkumar et al. 2013) by 62% (Manimaran et al.
71 2012), 48% (Sadeghinezhad et al. 2016) and 18.2% (Aly et al. 2017). Also, it was concluded
72 that some nanoparticles may deposit on the heat pipe wall making a coating resulting in an
73 increase of the surface wettability (Sadeghinezhad et al. 2016; Cheedarala et al. 2016).

74 On the other hand, some researchers have implemented different surface characteristics to enhance the
75 thermal performance of heat pipes. (Han & Cho 2002) investigated the performance of a micro-grooved
76 thermosyphon heat pipe for different working fluids, number of grooves and operating temperatures.
77 They found that the number of 60 grooves correspond to the highest condensation heat transfer
78 performance which was 2.5 times higher than that of a plain thermosyphon. Also, the condensation heat
79 transfer coefficients of grooved thermosyphons filled with methanol and ethanol were 1.5-2 and 1.3-
80 1.5 times higher compared to the plain one, respectively, and water provides the highest heat transfer
81 rate. The thermal characteristics of two thermosyphon heat pipes with straight and helical grooves filled
82 with water have been investigated by (Han & Cho 2005) for different inclinations, fill ratios and
83 operating temperatures. It is concluded that the fill ratio of 30% exhibits the highest heat flux. In
84 addition, angles of 25-30° and 40° provide the best thermal performance for helical and straight grooves,
85 respectively. (Jiao et al. 2005) studied theoretically and experimentally the effect of thin-film
86 evaporation in a groove heat pipe. They reported that the performance of the grooved heat pipe is highly
87 affected by the thin film evaporation where the reduction in evaporator temperature is considerably
88 larger than in condenser temperature. Also, the thin film region is enlarged by the decrease in the contact
89 angle which increases the heat transfer performance. A similar mathematical study to (Jiao et al. 2005)
90 has been carried out by (Jiao et al. 2007), but the thin fill region inside the groove was divided into three
91 different regions instead of one region. A numerical thermal model has been developed to predict the
92 thermal performance of a micro-grooved flat plate heat pipe and validated with an experimental study
93 (Lefèvre et al. 2008). They found that the optimum dimensions of the rectangular groove are 0.36, 0.7
94 and 0.1 mm corresponding to groove width, height and fin width, respectively. These dimensions
95 provide a maximum heat flux and lowest thermal resistance. (Yong et al. 2010) investigated the
96 performance of a heat pipe with micro-grooves manufactured by Extrusion-ploughing process. The
97 study reported that the heat transfer limit for the grooved heat pipe fabricated by the new technique is
98 larger than that for the normal grooved heat pipe, thus the low heat transfer limit for axially micro-
99 grooved heat pipe can be resolved. (Wong & Lin 2011) investigated the impact of surface wettability
100 on the performance of evaporator in a mesh wicked flat plate heat pipe with water, methanol and acetone
101 as working fluids. They concluded that the heat transfer limit decreases as the contact angle of the

102 copper surface with water increases, while it is unaffected by methanol and acetone. (Solomon et al.
103 2012) studied the effect of nanoparticles coating on the thermal performance of screen wick heat
104 pipe. Results revealed that the heat transfer coefficient and thermal resistance of the evaporator
105 increases and reduces by 40%, respectively, while the thermal performance in the condenser section
106 decreases compared with an uncoated heat pipe. It is also reported that reduction of 19%, 15%, and
107 14% is achieved at heat loads of 100, 150 and 200 W respectively. Thermal characteristics of a
108 horizontal grooved heat pipe with different surface wettability for the three sections, evaporator,
109 adiabatic and condenser has been investigated by (Hu et al. 2013). The study revealed that significant
110 decrease is achieved in the total thermal resistance due to the change to the surface characteristics to
111 hydrophilic, gradient wettability and normal surface for evaporator, adiabatic and condenser sections,
112 respectively. Also, more than 42% increase in the dry out limit of the grooved heat pipe is obtained.

113 (Rahimi et al. 2010) changed the surface characteristics of the evaporator and condenser to investigate
114 their influence on the thermal performance of a two-phase closed thermosyphon using water as a
115 working fluid. The study showed that the thermosyphon efficiency can be increased by 15.27%,
116 whereas a decrease of 2.35 times in the thermal resistance is obtained compared with the plain TPCT.

117 Another surface modification study has been carried out by (Solomon et al. 2013) to test the heat transfer
118 performance of an anodized Aluminium thermosyphon charged with acetone. It is found that a
119 maximum reduction in thermal resistance and increase in heat transfer coefficient of the TPCT
120 evaporator is 15% compared with non-anodized thermosyphon. In addition, a negligible effect of
121 anodized TPCT is observed on the condenser thermal performance. (Hsu et al. 2014) employed
122 different surface characteristics in terms of contact angle in the evaporator and condenser sections to
123 investigate the thermal performance of a TPCT. Experimental results showed that when evaporator and
124 condenser are superhydrophilic and superhydrophobic, respectively, the highest performance of the
125 TPCT is obtained where the maximum reduction in the thermal resistance is 26.1% compared with plain
126 one. Also, the worst thermal performance of the thermosyphon is observed when the whole inside wall
127 of the TPCT is superhydrophilic. The effect of internal helical microfin on the condensation heat
128 transfer performance in a TPCT has been investigated by (Wang et al. 2012). They reported that the

129 existence of the internal helical microfin provides a better thermal response and increases the heat
130 transfer coefficient of condensation by 116.87% at high heat load. Also, A correlation for predicting the
131 condensation heat transfer coefficient of the TPCT was proposed. (Nair & Balaji 2015) investigated
132 numerically using Fluent and Matlab the effect of internal fins inside the condenser section on the
133 performance of a two-phase closed thermosyphon. They concluded that adding 8 fins in the condenser
134 section increases the thermal conductivity of the TPCT by about 43%. It is also reported that additional
135 condensate mass of 22% and 32% can be produced using 8 and 12 fins, respectively, which would be
136 helpful to avoid the dry out during the operation of the thermosyphon. A similar study to (Nair & Balaji
137 2015) has been carried out experimentally by (Naresh & Balaji 2017), but for various fill ratios and two
138 working fluids, water and acetone. They concluded that at low heat load, reduction of 17% and 35.48%
139 is obtained in the temperature and thermal resistance of TPCT due additional condensate mass resulting
140 from inserting six internal fins in the condenser section. It is also reported that the optimum thermal
141 performance of the TPCT is achieved at a fill ratio of 50%. In addition, acetone exhibits higher
142 performance at low heat loads, while water provides better performance at high heat inputs.

143 Many researchers have carried out numerous experimental investigations to enhance the thermal
144 performance and increase the heat transfer limit of heat pipes. This has been achieved by implementing
145 different means namely, using nanoparticles to improve the thermal characteristics of fluids or changing
146 the surface features of the wall using coatings or making micro-grooves. However, the preparation and
147 using of nanofluids would be complex and occupied by instability and agglomeration of the
148 nanoparticles. In addition, surface coatings can be a difficult process, making additional conduction
149 thermal resistance, time-consuming and expensive, whereas making micro-grooves may reduce the
150 boiling heat transfer limit of heat pipes.

151 In contrast, making a roughness on the internal wall of a TPCT implementing a new technique does not
152 need any use of such additional coatings or materials. This would produce an effective energy
153 conversion device that can be used in many applications. Therefore, the objective of this work is to
154 enhance the thermal performance of thermosyphon heat pipe by making an internal wall roughness
155 employing a new advanced machining technique named as Electrical Discharge Machining (EDM). To

156 achieve this goal, a copper tube was machined to make the wall roughness, manufactured and tested to
157 compare its thermal performance with a plain copper thermosyphon at two different initial sub-
158 atmospheric pressures (3 and 30 *kPa*) and various heat loads.

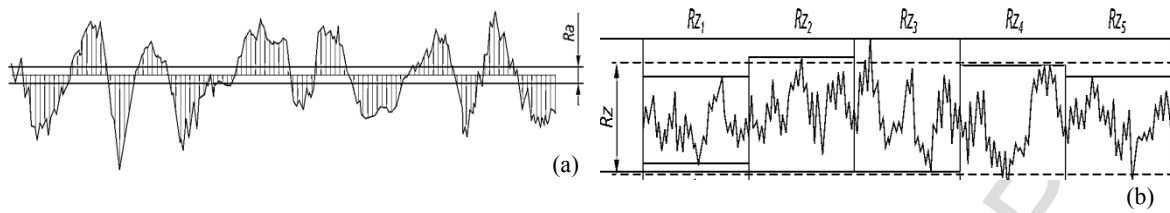
159 **2.Experimental work**

160 **2.1. Manufacture of the rough surface**

161 Electrical Discharge Machining (EDM) or Spark Erosion Machining (SEM) was used to make a surface
162 roughness inside a tube with a 200 mm length, 12.7 mm outside diameter and 1.6 mm thickness. This
163 machine generates an electrical spark between a cutting wire (electrode) and a sample material. The
164 spark indicates the flowing of the electrical power through the wire. Thus, the material (workpiece)
165 starts melting due to the intensively produced heat which produces a very high temperature. The spark
166 is controlled and positioned cautiously in order to machine only the material surface. Deionized water
167 is always used as a dielectric medium for the spark in the case of the wire EDM. Water not only
168 functions as a coolant but also to remove the eroded material away from the surface. The wire diameter
169 is between 0.1-0.3 mm and is made either from brass or copper. Also, the electrode (wire) must not be
170 in direct contact with the sample material and the workpiece must be electrically conductive. The
171 minimum eroded thickness is 0.00254 mm and the maximum is 0.051 mm per one pass (Johnson
172 Waukesha).

173 The resulting roughness was measured using Mitutoyo Surftest SJ-310 tester in terms of two
174 parameters. The first is *Ra* which represents the average distance between the peaks and valleys and the
175 deviation from the mean line throughout the surface and along the length of the surface. The second is
176 *Rz* which represents the average of five sampling lengths by indicating the vertical distance between
177 the highest peak and the deepest valley for each sampling length. The two roughness parameters *Ra* and
178 *Rz* are illustrated in Fig.1a and Fig.1b, respectively. The surface roughness was measured at five
179 different positions on the sample surface, Table 1 illustrates these values. Also, two actual zoomed
180 photos for rough and plain surfaces are presented in Fig.2a and Fig.2b, respectively. To report the
181 wettability of the two surfaces, an optical tensiometer-contact angle meter was used to measure the

182 contact angle employing the sessile drop technique. The measured contact angles for the rough and
 183 plain surfaces are shown in Fig.3a and Fig.3b, respectively.



184

185 Fig.1 Sketch shows: (a)- R_a , arithmetical mean roughness and (b)- R_z , mean roughness depth

186

187

188

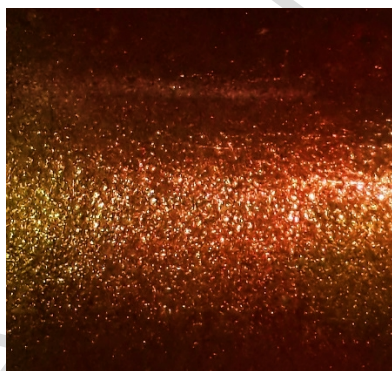
189

Table 1. Values of R_a and R_z

Item	Rough surface		Plain surface	
	R_a (μm)	R_z (μm)	R_a (μm)	R_z (μm)
1	2.935	15.256	0.289	1.89
2	3.658	22.268	0.278	1.764
3	3.675	20.460	0.275	1.687
4	3.664	21.568	0.275	1.67
5	3.639	21.376	0.281	1.82

190

191



192

193

194

Fig.2a Rough copper surface

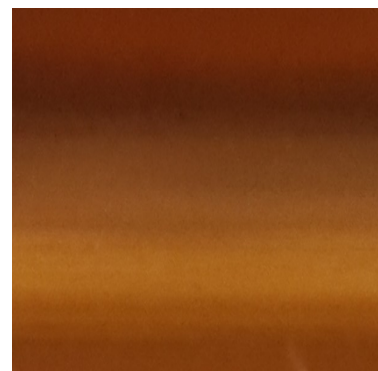


Fig.2b Plain copper surface

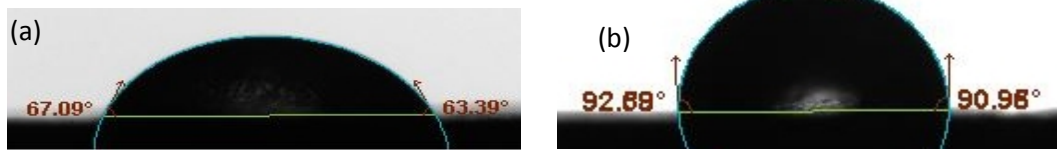
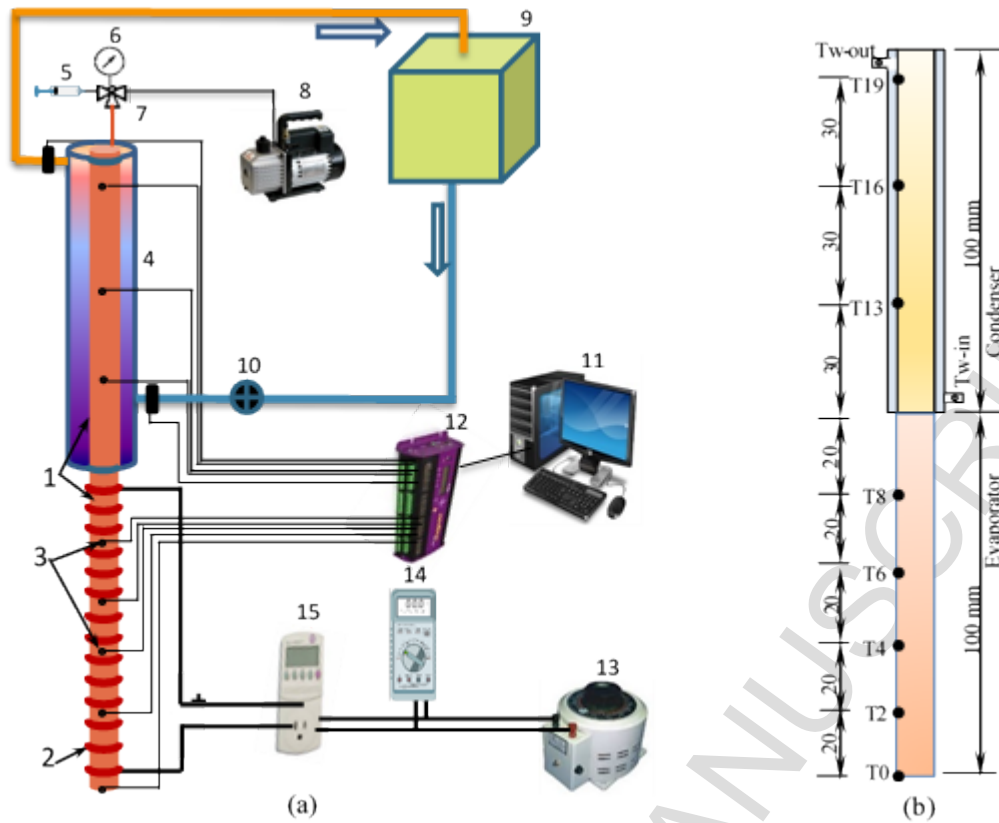


Fig.3 Measured contact angle for: (a) Rough and (b) plain copper surfaces

2.2. Test set up and procedure

An experimental apparatus was developed to investigate the effect of the surface roughness on the heat transfer performance of the TPCT at a range of heat inputs and two initial pressures.

After the roughness was made on the entire internal wall of the TPCT, the resulting rough tube and another plain copper tube were employed to fabricate two thermosyphon heat pipes. The process starts by rinsing the two tubes many times with the ethanol to remove any grease or other Contaminants, then washing with deionised water to ensure that all ethanol was removed. After that, the two proposed thermosyphons were evacuated to a desired pressure (3 kPa or 30 kPa) using a vacuum pump, then they were charged with deionised water to fill the half of the evaporator (50%) using a syringe as shown in Fig.4a. The thermosyphon is 200 mm long and consists of two sections, the evaporator and condenser with 100 mm length each, 12.7 mm outside diameter and 1.6 mm thickness. The condenser section is surrounded by a brass water jacket of 16 mm inside diameter and 28 mm outside diameter to remove the heat from the condenser using water as a cooling liquid. Eight type T surface thermocouples were fixed on the outer surface of the TPCT to measure the wall temperature, five thermocouples at the evaporator and three at the condenser. In addition, two type T probe thermocouples were fitted in the inlet and outlet of the water jacket to measure the inlet and outlet temperatures of the cooling water. Before using the thermocouples, All the ten thermocouples were immersed in water at a constant temperature to be calibrated with an RTD thermocouple where the maximum deviation from the RTD reading was found to be $\pm 0.4^{\circ}\text{C}$ at steady state. Fig.4b illustrates the TPCT dimensions and the positions of thermocouples.



218

219 1-Heat pipe, 2-Electrical heater, 3-Thermocouples positions, 4- Water jacket, 5-Syringe, 6-Pressure gauge, 7-Three-way valve, 8-Vacuum
 220 pump, 9-Constant temperature water bath, 10- Flow meter 11-Computer, 12-Data logger, 13-Variable transformer, 14-Multimeter, 15-Power
 221 meter.

222 Fig.4: (a)- Test rig schematic diagram and (b)- Dimensions and thermocouples positions

223

224 An electrical heater with a maximum power of 160 W was used to supply the heat to the evaporator
 225 section where it was wrapped evenly to distribute the heat input equally on the evaporator surface.

226 Consequently, the value of the heat input applied to the evaporator wall can be changed by changing

227 the input voltage using a variable transformer. Also, a wattmeter and multimeter were used to measure

228 the heat load. Comparing the readings of the wattmeter, multimeter (volt and ampere) and the value of

229 the output heat, it is found that the maximum uncertainty in the input energy is about 3.2%. A high-

230 temperature superwool blanket insulation of 50 mm thickness was used to reduce the thermal losses

231 from the evaporator wall of the TPCT, so, the heat losses were neglected. This was also proved by

232 comparing the heat output which was found to be more than 93% in all tests. Also, a rotameter was

233 employed to measure the coolant mass flow rate at the condenser section with the uncertainty of

234 measuring the flow rate value of 2.8%. In addition, to ensure that all tests are performed at the same

235 inlet temperature of the cooling water, a constant temperature water bath was used to maintain the

236 coolant inlet temperature at the desired temperature. All thermocouples were connected to a data taker
237 to send their temperature readings into a computer to be saved and analysed.

238 After the test rig was built, it was ready to examine the TPCT performance. Firstly, the water bath is set
239 at a desired cooling temperature (20°C). Then, the globe valve before the rotameter is opened to allow
240 the cooling water to circulate throughout the water jacket at the condenser section. Also, the rotameter
241 is adjusted to a specified flow rate of 0.0025 kg/s using the globe valve to be fixed for all tests. Before
242 power is supplied to the rope heater, enough time is provided to ensure that all thermocouples readings
243 reach approximately a value of 20°C which is another proof of thermocouples consistency and accuracy
244 in temperature measurement. Then, the power is supplied to the electrical heater by adjusting the
245 variable transformer to a certain value which equivalent to the desired heat input needed to the
246 evaporator section. This heat input can be obtained by multiplying the voltage times the current as well
247 as the reading of the wattmeter. After all temperatures reach the steady state, the data is saved and the
248 power is switched off. Some runs were repeated three times to prove the repeatability and accuracy of
249 the test facility and the procedure used. The measured quantities are the heat load, operating pressure,
250 coolant mass flow rate, inlet and outlet temperatures of the cooling water and wall temperatures of the
251 evaporator and condenser sections.

252

253

254 **2.3. Data reduction**

255 Parameters such as evaporator and condenser thermal resistances, total thermal resistance and the
256 evaporator heat transfer coefficient need to be determined to obtain and compare the heat transfer
257 characteristics of the plain and modified TPCTs.

258 The evaporator and condenser thermal resistances can be obtained from the following equations:

$$259 \quad R_e = \frac{T_{e,av} - T_{sat}}{Q} \dots\dots\dots(1)$$

$$260 \quad R_c = \frac{T_{c,av} - T_{sat}}{Q} \dots\dots\dots(2)$$

261 Where R_e and R_c are the evaporator and condenser thermal resistances, respectively, T_{sat} is the
 262 saturation temperature which corresponds to operating pressure at each heat input, and Q is the heat
 263 input calculated from:

$$264 \quad Q = IV \dots\dots\dots(3)$$

265 Where I and V are the circuit current and voltage, respectively.

266 $T_{e,av}$ and $T_{c,av}$ are the average wall temperatures of the evaporator and condenser, respectively and can
 267 be obtained as follow:

$$268 \quad T_{e,av} = \frac{T_0 + T_2 + T_4 + T_6 + T_8}{5} \dots\dots\dots(4)$$

$$269 \quad T_{c,av} = \frac{T_{13} + T_{16} + T_{19}}{3} \dots\dots\dots(5)$$

270 Therefore, the total thermal resistance of the TPCT can be calculated from:

$$271 \quad R_t = \frac{T_{e,av} - T_{c,av}}{Q} \dots\dots\dots(6)$$

272 Where R_t is the total thermal resistance of the thermosyphon.

273 The evaporator heat transfer coefficient can be obtained from the following equation:

$$274 \quad h_e = \frac{Q}{\pi D_i L_e (T_{i,av} - T_{sat})} \dots\dots\dots(7)$$

275 Where h_e is the evaporator heat transfer coefficient, D_i and L are the inside diameter and length of the
 276 evaporator and $T_{i,av}$ is the inside surface average temperature of the evaporator and can be determined
 277 from:

$$278 \quad T_{i,av} = T_{e,av} - \frac{Q}{2\pi L K} \ln\left(\frac{D_o}{D_i}\right) \dots\dots\dots(8)$$

279 Where D_o is the outside diameter of the evaporator and K is the solid thermal conductivity.

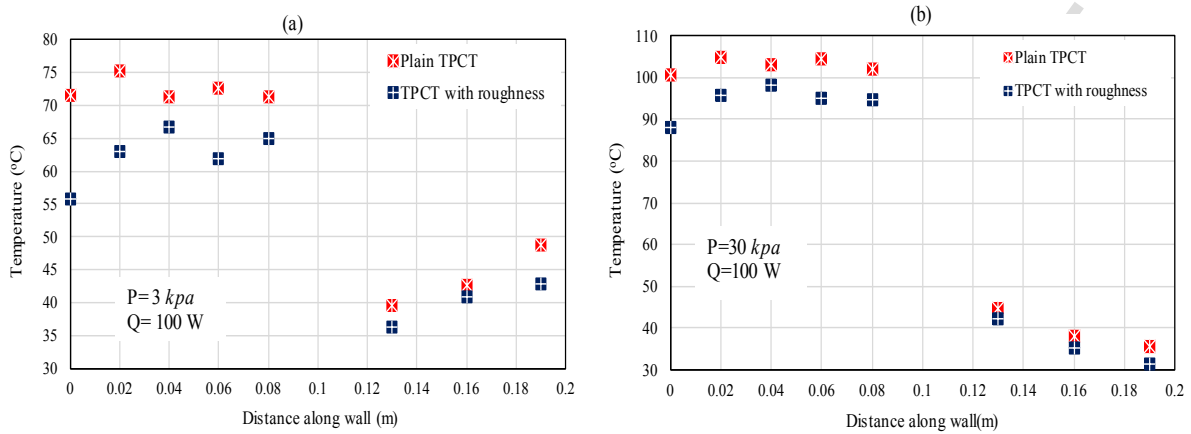
280 3- Results and discussion

281 3.1. Temperature distribution

282 A TPCT with internal wall roughness made using the EDM technique was tested and compared
283 with a smooth TPCT to investigate the enhancement in the heat transfer at a range of heat loads
284 and two different initial pressures.

285 Variation of the wall temperature of the plain and rough thermosyphons with distance along the wall at
286 a heat load of 100 W is shown in Fig.5a and Fig.5b for initial pressures of 3 and 30 kPa, respectively.
287 Fig. 5a shows that a significant reduction in the evaporator wall temperature is achieved for the TPCT
288 with roughness compared to the plain TPCT. This can be explained by the increase in the nucleation
289 sites density (as confirmed by Fig. 2a), thereby increasing the frequency of bubbles generation
290 (Solomon et al. 2013) resulting from a rough surface, which transfers heat efficiently from the TPCT
291 wall reducing noticeably the wall temperature. Another reason causing the decrease in the evaporator
292 wall temperature is the hydrophilic characteristics of the modified wall [25, 27] which make the surface
293 wetted with liquid instead of vapour as illustrated in Fig.3a. However, in the condenser section, it is
294 observed that the condenser wall temperature of the plain TPCT is higher than that for the TPCT with
295 roughness, but the difference is much lower compared with the evaporator. This also may be attributed
296 to the wettability feature of the rough surface which provides opposite effect on the condensation heat
297 transfer in the condenser. This results in increasing the condensate film thickness which leads to
298 additional heat transfer resistance, thereby lower condenser wall temperature. Fig.5b presents a similar
299 trend as Fig.5a in the evaporator section for both plain and modified TPCTs. However, a lower
300 difference in evaporator temperature is obtained between the two thermosyphons due to the higher
301 pressure. The reason behind that may be attributed to the activation of small surface cavities of the plain
302 TPCT when the pressure increases (Khodabandeh & Palm 2002) which reduces the wall temperature
303 of the plain TPCT. On the other hand, most cavities of the rough surface are already activated, so the
304 increase in pressure produces relatively less temperature reduction compared with the plain TPCT, but
305 the evaporator wall temperature of the rough TPCT is still lower than that of the plain TPCT due to the

306 roughness effect. Also, a different trend of the condenser wall temperature is observed at a pressure of
 307 30 kPa compared with that at 3 kPa for both TPCTs. The reason will be explained in the discussion of
 308 Fig.7a and b.



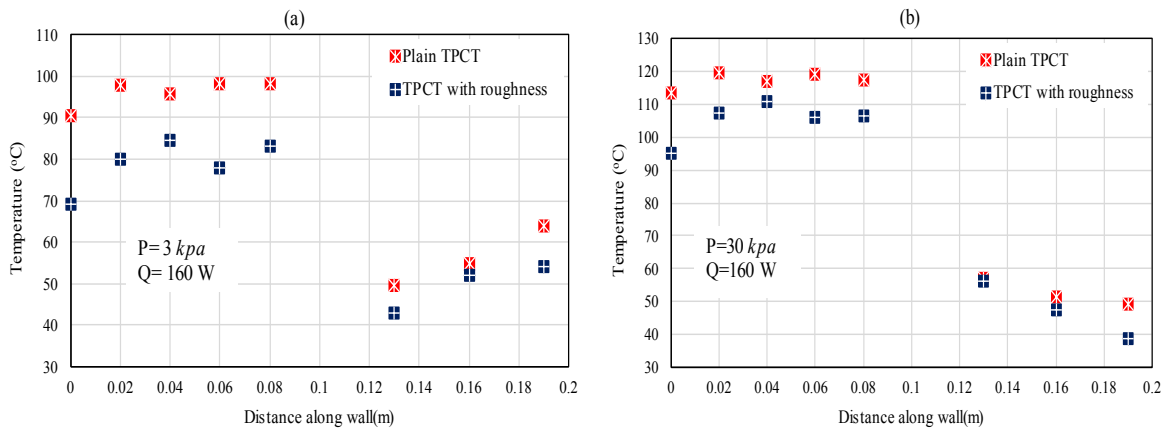
309

310 Fig.5 Comparison of thermosyphon wall temperature between plain and rough TPCT at heat load 100 W and
 311 initial pressures: (a)-3 kPa and (b)-30 kPa

312

313 Figs.6a and b also show the temperature distribution along the wall of the two TPCTs at 3 and 30 kPa,
 314 respectively, but at a heat input of 160 W. It is observed that the difference in the evaporator wall
 315 temperature between the plain and modified thermosyphons is higher compared with that at a heat load
 316 of 100 W. This could be explained as: before reaching the critical heat flux, when the heat load
 317 increases, the heat transfer mechanism is enhanced due to the generation of more bubbles transferring
 318 further heat from the heating surface to the fluid, thereby further reduces the evaporator wall
 319 temperature. On the other hand, approximately the same difference in the condenser wall temperature
 320 as in the case of 100 W is obtained when the pressure is 3 kPa (Fig.6a). However, when the pressure is
 321 30 kPa (Fig.6b), a higher difference in the wall temperature of the condenser is noticed between the two
 322 TPTCs compared with that at 100 W, especially at the upper part of the rough thermosyphon. This can
 323 be explained that the rate at which the vapour is generated at 160 W is higher than that at 100 W in both
 324 plain and rough TPCTs. Therefore, the rate of the condensate removal is smaller than the rate of droplets
 325 growth, which leads to thickening the condensate film thus reducing the condenser wall temperature
 326 (Attinger et al. 2014). This effect is higher in the case of the rough condenser due to the wettable

327 characteristics of the rough surface compared with the smooth surface, so that the difference at 160 W
 328 is higher than that at 100 W.



329

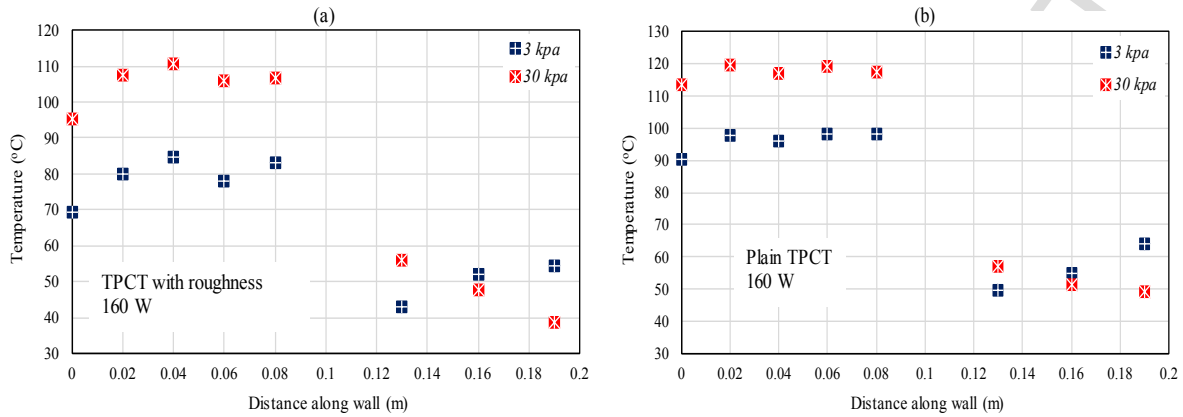
330 Fig.6 Comparison of thermosyphon wall temperature between plain and rough TPCT at heat load 160 W and
 331 initial pressures: (a)-3 kPa and (b)-30 kPa

332

333 Effect of two initial pressures of 3 and 30 kPa on the wall temperature distribution is presented in Fig.7a
 334 and Fig.7b for rough and plain thermosyphons, respectively, at a heat input of 160 W. It can be seen
 335 that for both TPCTs, using the pressure of 3 kPa provides a lower evaporator wall temperature compared
 336 with 30 kPa due to corresponding low saturation temperature which leads to earlier evaporation start-
 337 up, thereby a lower evaporator wall temperature (Yang et al. 2008), (Lee et al. 2014). On the other
 338 hand, a higher condenser wall temperature is obtained employing 3 kPa at the middle and upper parts
 339 of the condenser (T16 and T19), while it is lower at the lower part (T13). This may result from the rising
 340 of the saturated vapour to the upper part of the condenser and the small condensate film thickness,
 341 resulting in a low thermal resistance, thereby higher heat transfer coefficient between the hot vapour
 342 and the wall leading to a higher condenser wall temperature at the upper part compared with the lower
 343 part (Alizadehdakhel et al. 2010). In contrast, in the case of 30 kPa, the upper part of the condenser wall
 344 exhibits a lower wall temperature compared to the lower part for both TPCTs. This may be attributed
 345 to the presence of non-condensable gases in the case of 30 kPa which blocks the upper part of the
 346 condenser preventing the hot vapour to reach this part and deteriorating the heat transfer mechanism
 347 leading to a lower condenser wall temperature compared with the lower part at 3 kPa. Thus, a smaller
 348 condensate quantity is produced making the wall temperature of the lower part of the condenser (T13)

349 for both TPCTs at 30 kPa higher than that at 3 kPa. In addition, the difference in the wall temperature
 350 between the two pressures is higher in the case of modified TPCT compared with plain one for the same
 351 reasons explained in the discussion of Fig.5a-b and Fig.6a-b.

352



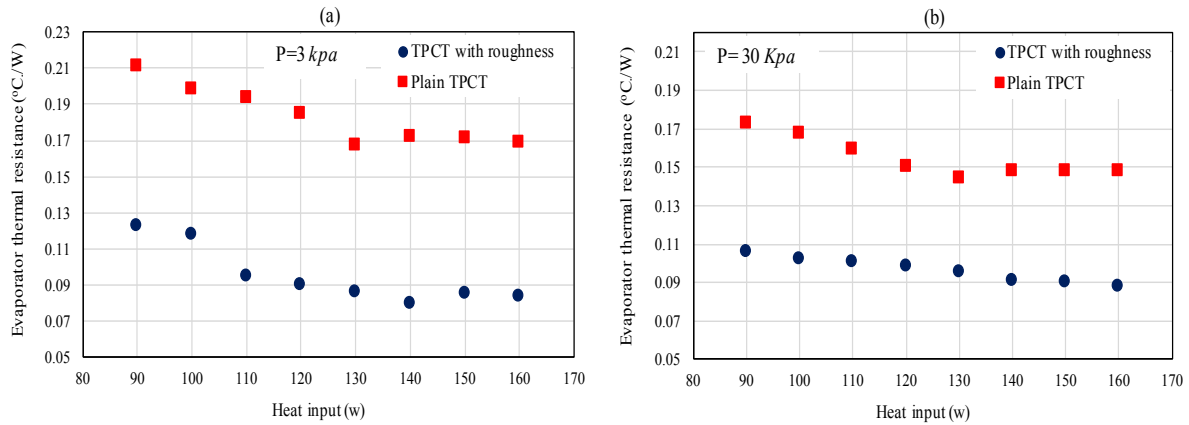
353

354 Fig.7 Comparison of thermosyphon wall temperature between initial pressures 3 and 30 kPa at heat load 160 W
 355 and: (a)-TPCT with roughness and (b)-Plain TPCT

356

357 3.2. Thermal performance of the Thermosyphon

358 Variation of evaporator thermal resistance (R_e) with the heat load for the plain and rough TPCTs are
 359 shown in Fig.8a and Fig.8b at two different initial pressures of 3 and 30 kPa, respectively. They show
 360 that a considerable decrease in the evaporator thermal resistance is achieved when the rough
 361 thermosyphon is used compared with the plain one for both pressures. It is found that the reduction in
 362 the evaporator thermal resistance varies with the heat load from about 51-68% and from 68-115% for
 363 pressures of 30 and 3 kPa, respectively (30.4% (Aly et al. 2017), 40% (Solomon et al. 2012), 15.01%
 364 (Solomon et al. 2013)). This reduction in R_e may result from the presence of the roughness in the
 365 evaporator wall which creates additional nucleation sites leading to generate more bubbles, thereby
 366 more heat is released from the evaporator internal surface. Also, the rough surface increases the wall
 367 wettability by decreasing the contact angle making the liquid in continuous contact with the evaporator
 368 wall removing the vapour away from the wall surface. In addition, it is observed that the R_e for the plain
 369 TPCT increases at a heat input of 140 W, while for the TPCT with roughness, it increases at 150 W
 370 indicating an increase in the CHF for the rough TPCT.

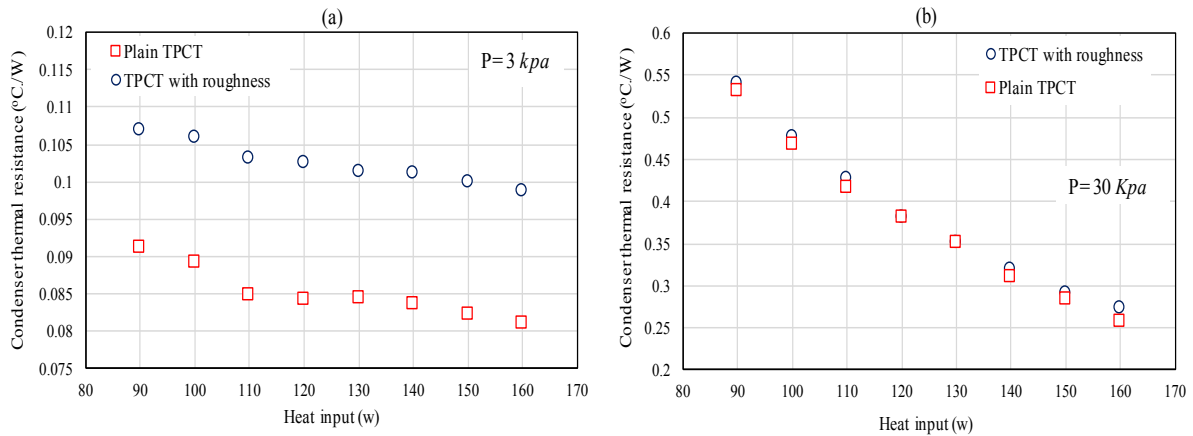


371

372 Fig.8 Comparison of evaporator thermal resistance versus heat input between plain and rough TPCTs at initial
 373 pressures: (a)-3 kPa and (b)-30 kPa

374

375 However, Fig.9a and Fig.9b show that the condenser thermal resistance (R_c) increases when the
 376 modified TPCT is employed compared with the plain one which worsens the heat transfer performance
 377 in the condenser section ((Solomon et al. 2012) also reported higher R_c for coated TPCT and (Solomon
 378 et al. 2013) reported no reduction in R_c for anodised TPCT). This may be attributed to the fact that the
 379 high surface wettability produced from the rough surface can form a liquid film on the condenser wall
 380 which prevents the vapour to be in direct contact with the condenser inner wall resulting in additional
 381 thermal resistance. The maximum increase in the R_c is about 22% compared with plain TPCT. It is also
 382 seen from Fig.9a 3 kPa initial pressure that R_c of the rough and plain TPCTs decreases steadily with the
 383 heat load, while Fig.9b for initial pressure of 30 kPa shows that R_c of both TPCTs decrease sharply with
 384 the heat load. This may be explained by a larger amount of vapour generated at the low pressure
 385 compared with the high pressure. This increases the liquid film thickness, thereby the condenser thermal
 386 resistance reducing the effect of heat input on the thermal resistance at the low pressure. The film
 387 thickness on the rough wettable condenser wall is higher (at 3 kPa), so that a higher difference is noticed
 388 between the two thermal resistances at a pressure of 3 kPa (Fig.9a) compared with that at 30 kPa
 389 (Fig.9b) and they both decrease with the input energy.

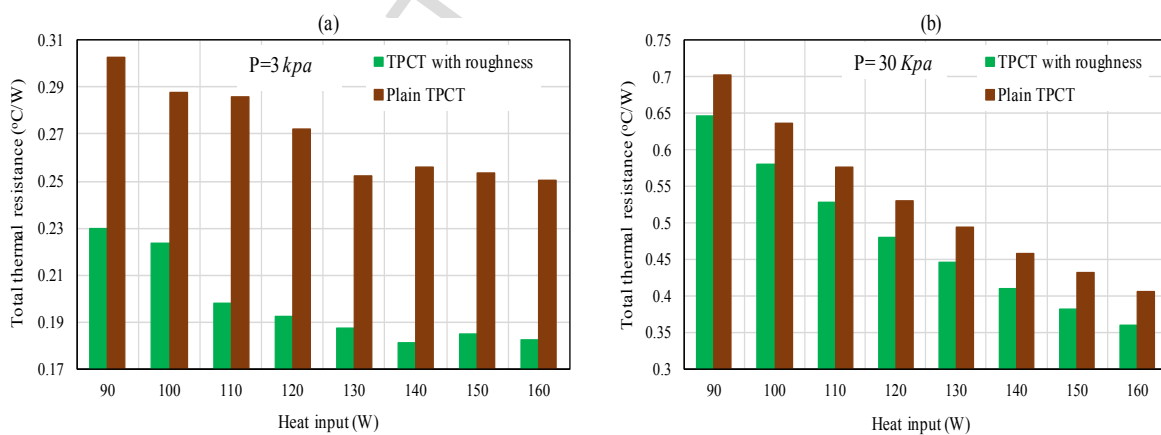


390

391 Fig.9 Comparison of condenser thermal resistance versus heat input between plain and rough TPCTs at initial
 392 pressures: (a)-3 kPa and (b)-30 kPa.

393

394 Despite the increase in condenser thermal resistance for the rough TPCT, a noticeable decrease in the
 395 total thermal resistance (R_t) of the rough TPCT is shown in Fig.10a and Fig.10b at 3 and 30 kPa,
 396 respectively, due to the high reduction in the evaporator thermal resistance. The reduction in the R_t
 397 varies with the input energy from about 9-13% and 28-42% compared with the plain TPCT at 30 and 3
 398 kPa respectively (18.2% (Aly et al. 2017), 19% (Solomon et al. 2012), 125% (Rahimi et al. 2010), 15%
 399 (Solomon et al. 2013), 26.1% (Hsu et al. 2014), 35.48% (Naresh & Balaji 2017)). In addition, Fig.10a
 400 (3 kPa) shows a same trend as the R_e in Fig.8a, and almost a same rate of decrease in the R_t for both
 401 TPCTs with the heat load is observed at a pressure of 30 kPa (Fig.10b).



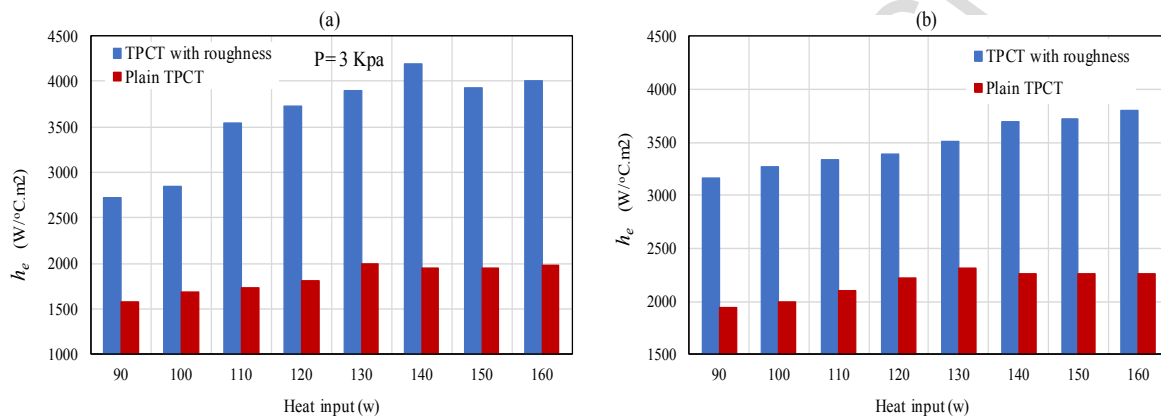
402

403 Fig. 10 Comparison of total thermal resistance versus heat input between plain and rough TPCTs at initial
 404 pressures: (a)-3 kPa and (b)-30 kPa.

405

406 Fig. 11a and Fig.11b show a significant enhancement in the evaporator heat transfer coefficient (h_e) for
 407 the TPCT with roughness at 3 and 30 kPa, respectively. The increase in the h_e is about 68-115% and

408 51-68% at 3 and 30 kPa, respectively (40% (Solomon et al. 2012), 50-100% for methanol and 30-50%
 409 for ethanol (Han & Cho 2002), maximum of 116.87% (Wang et al. 2012)). In addition, at a pressure of
 410 3 kPa (Fig.11a), h_e generally increases as the heat load increases for the both TPCTs. However, the rate
 411 of increase in h_e is higher for the modified TPCT compared with the plain one and it becomes
 412 approximately constant after a heat load of 130 W for the plain TPCT. Therefore, the difference in h_e
 413 between the two TPCTs increases as the input energy increases. This is also true at a pressure of 30 kPa
 414 (Fig.11b), but with a lower difference in h_e and a lower rate of increase for the rough TPCT.



415
 416 Fig.11 Comparison of evaporator heat transfer coefficient versus heat input between plain and rough TPCTs at
 417 initial pressures: (a)-3 kPa and (b)-30 kPa.

418

419 4- Conclusions

420 Thermal performance of a TPCT with an internal surface roughness produced using a new
 421 technique of EDM was tested to investigate the enhancement of heat transfer characteristics.
 422 This was carried out by comparing the modified TPCT with a plain TPCT at various heat loads
 423 and two different initial pressures (sub-atmospheric pressures). It is concluded that a significant
 424 decrease in the evaporator wall temperature is achieved using the resurfaced thermosyphon at
 425 both initial pressures 3 and 30 kPa. It is also seen that the reduction increases as the input
 426 energy increases. In addition, less reduction is obtained at a pressure of 30 kPa compared with
 427 3 kPa and the difference in $T_{e,av}$ between the two pressures for the rough TPCT is higher than
 428 that for the plain. Accordingly, a considerable decrease in the evaporator thermal resistance

429 and enhancement in the evaporator heat transfer coefficient of 115% and 68% are obtained at
430 3 and 30 kPa, respectively. However, the condenser wall temperature for the rough TPCT is
431 noticed to be lower than that for the plain one. Likewise, the thermal resistance of the condenser
432 section for the rough TPCT is higher, but the difference in the condenser much lower than that
433 at the evaporator. Thus, the total thermal resistance for modified TPCT is decreased by about
434 42% at a pressure of 3 kPa, whereas it is reduced by 13% at 30 kPa compared with the plain
435 TPCT despite the increase in the condenser thermal resistance. More enhancement in the
436 performance of the TPCT may be achieved if another proved enhanced surface is employed in
437 the condenser rather than the rough surface or using a nanofluid such as Ti/H₂O which was
438 proved to enhance the h_c by 2-3 times (Baojin et al. 2009) with the rough TPCT. This may need
439 to be investigated by a further research study and can be included as a future question: how can
440 enhance the heat transfer characteristics in the condenser to achieve more enhancement in the
441 thermal performance of the TPCT?

442 Therefore, making a roughness in the internal wall surface of the TPCT using EDM provides
443 a simple and inexpensive technique to enhance the heat transfer performance of the TPCT. This
444 would offer an efficient energy conversion and heat removal device for different systems in
445 many applications.

446

447 **Acknowledgement**

448 The first author would like to acknowledge the Iraqi Ministry of Higher Education and
449 Scientific Research and Ministry of Electricity for sponsoring this Work.

450

451 **References**

452 Alammari, A.A., Al-Dadah, R.K. & Mahmoud, S.M., 2017. Experimental investigation of the
453 influence of the geyser boiling phenomenon on the thermal performance of a two-phase closed
454 thermosyphon. *Journal of Cleaner Production*, 172, pp.2531–2543. Available at:
455 <https://doi.org/10.1016/j.jclepro.2017.11.157>.

456 Alizadehdakhel, A., Rahimi, M. & Alsairafi, A.A., 2010. CFD modeling of flow and heat transfer in a

- 457 thermosyphon. *International Communications in Heat and Mass Transfer*, 37(3), pp.312–318.
- 458 Aly, W.I.A. et al., 2017. Thermal performance evaluation of a helically-micro-grooved heat pipe
459 working with water and aqueous Al₂O₃ nanofluid at different inclination angle and filling ratio.
460 *Applied Thermal Engineering*, 110, pp.1294–1304. Available at:
461 <http://dx.doi.org/10.1016/j.applthermaleng.2016.08.130>.
- 462 Attinger, D. et al., 2014. Surface engineering for phase change heat transfer: A review. *MRS Energy
463 & Sustainability*, 1, p.E4. Available at:
464 http://www.journals.cambridge.org/abstract_S2329222914000099.
- 465 Baojin, Q. et al., 2009. Heat transfer characteristics of titanium/water two-phase closed
466 thermosyphon. *Energy Conversion and Management*, 50(9), pp.2174–2179. Available at:
467 <http://dx.doi.org/10.1016/j.enconman.2009.04.030>.
- 468 Cheedarala, R.K. et al., 2016. Experimental study on critical heat flux of highly efficient soft
469 hydrophilic CuO–chitosan nanofluid templates. *International Journal of Heat and Mass
470 Transfer*, 100, pp.396–406. Available at:
471 <http://linkinghub.elsevier.com/retrieve/pii/S0017931015305846>.
- 472 Ghanbarpour, M. et al., 2015. Thermal performance of inclined screen mesh heat pipes using silver
473 nanofluids. *International Communications in Heat and Mass Transfer*, 67, pp.14–20. Available
474 at: <http://dx.doi.org/10.1016/j.icheatmasstransfer.2015.06.009>.
- 475 Han, K. & Cho, D.-H., 2005. A comparison of the heat transfer performance of thermosyphon using a
476 straight groove and a helical groove. *Journal of Mechanical Science and Technology*, 19(12),
477 pp.2296–2302.
- 478 Han, K. & Cho, D.-H., 2002. Effect of micro groove on the performance of condensing heat transfer
479 of the micro grooved thermosyphon. *International Journal of Air-Conditioning and
480 Refrigeration*, 10(4), pp.184–191.
- 481 Hsu, C. et al., 2014. Thermal Performance Improvement of a Cylindrical Thermosyphon with
482 Modified Wettability on both Evaporator and Condenser Sections. *American Journal of Heat
483 and Mass Transfer*, 1(2), pp.81–89.
- 484 Hu, Y. et al., 2013. Thermal performance enhancement of grooved heat pipes with inner surface
485 treatment. *International Journal of Heat and Mass Transfer*, 67, pp.416–419. Available at:
486 <http://dx.doi.org/10.1016/j.ijheatmasstransfer.2013.08.035>.
- 487 Huminic, G. et al., 2011. Experimental study of the thermal performance of thermosyphon heat pipe
488 using iron oxide nanoparticles. *International Journal of Heat and Mass Transfer*, 54(1–3),
489 pp.656–661. Available at: <http://dx.doi.org/10.1016/j.ijheatmasstransfer.2010.09.005>.
- 490 Huminic, G. & Huminic, A., 2013. Numerical study on heat transfer characteristics of thermosyphon
491 heat pipes using nanofluids. *Energy Conversion and Management*, 76, pp.393–399. Available at:
492 <http://dx.doi.org/10.1016/j.enconman.2013.07.026>.
- 493 Jiao, A.J. et al., 2005. Thin film evaporation effect on heat transport capability in a grooved heat pipe.
494 *Microfluidics and Nanofluidics*, 1(3), pp.227–233. Available at:
495 <http://link.springer.com/10.1007/s10404-004-0015-6>.
- 496 Jiao, A.J., Ma, H.B. & Critser, J.K., 2007. Evaporation heat transfer characteristics of a grooved heat
497 pipe with micro-trapezoidal grooves. *International Journal of Heat and Mass Transfer*, 50(15–
498 16), pp.2905–2911.
- 499 Johnson Waukesha, How EDM works. Available at: [https://www.xactedm.com/edm-capabilities/how-
500 edm-works/](https://www.xactedm.com/edm-capabilities/how-edm-works/) [Accessed December 21, 2017].
- 501 Jouhara, H. et al., 2017. Heat pipe based systems - Advances and applications. *Energy*, 128, pp.729–

- 502 754. Available at: <http://dx.doi.org/10.1016/j.energy.2017.04.028>.
- 503 Khodabandeh, R. & Palm, B., 2002. Influence of system pressure on the boiling heat transfer
504 coefficient in a closed two-phase thermosyphon loop ☆. , 41, pp.619–624.
- 505 Lee, C.Y. et al., 2014. Numerical simulation of the heat transfer characteristics of low-watt
506 thermosyphon influence factors. *Journal of Applied Science and Engineering*, 17(4), pp.423–
507 428.
- 508 Lefèvre, F. et al., 2008. Prediction of the temperature field in flat plate heat pipes with micro-grooves
509 – Experimental validation. *International Journal of Heat and Mass Transfer*, 51(15–16),
510 pp.4083–4094. Available at:
511 <http://www.sciencedirect.com/science/article/pii/S0017931007007466>.
- 512 Liu, Z.H., Li, Y.Y. & Bao, R., 2010. Thermal performance of inclined grooved heat pipes using
513 nanofluids. *International Journal of Thermal Sciences*, 49(9), pp.1680–1687. Available at:
514 <http://dx.doi.org/10.1016/j.ijthermalsci.2010.03.006>.
- 515 Manimaran, R., Palaniradja, K. & Alagumurthi, N., 2012. Effect of filling ratio on thermal
516 characteristics of circular heat pipe using nanofluid. *Frontiers in Heat Pipes*, 3(2), pp.1–5.
- 517 Nair, R.S. & Balaji, C., 2015. Synergistic analysis of heat transfer characteristics of an internally
518 finned two phase closed thermosyphon. *Applied Thermal Engineering*, 101, pp.720–729.
519 Available at: <http://dx.doi.org/10.1016/j.applthermaleng.2016.01.084>.
- 520 Naresh, Y. & Balaji, C., 2017. Experimental investigations of heat transfer from an internally finned
521 two phase closed thermosyphon. *Applied Thermal Engineering*, 112, pp.1658–1666. Available
522 at: <http://dx.doi.org/10.1016/j.applthermaleng.2016.10.084>.
- 523 Noie, S.H. et al., 2009. Heat transfer enhancement using Al₂O₃/water nanofluid in a two-phase closed
524 thermosyphon. *International Journal of Heat and Fluid Flow*, 30(4), pp.700–705. Available at:
525 <http://dx.doi.org/10.1016/j.ijheatfluidflow.2009.03.001>.
- 526 Paramatthanuwat, T. et al., 2010. Heat transfer characteristics of a two-phase closed thermosyphon
527 using de ionized water mixed with silver nano. *Heat Mass Transfer*, 46, pp.281–285.
- 528 Rahimi, M., Asgary, K. & Jesri, S., 2010. Thermal characteristics of a resurfaced condenser and
529 evaporator closed two-phase thermosyphon. *International Communications in Heat and Mass
530 Transfer*, 37(6), pp.703–710. Available at:
531 <http://dx.doi.org/10.1016/j.icheatmasstransfer.2010.02.006>.
- 532 Sadeghinezhad, E. et al., 2016. Experimental investigation of the effect of graphene nanofluids on
533 heat pipe thermal performance. *Applied Thermal Engineering*, 100, pp.775–787. Available at:
534 <http://linkinghub.elsevier.com/retrieve/pii/S1359431116302149>.
- 535 Shanbedi, M. et al., 2012a. Investigation of heat-transfer characterization of EDA-MWCNT/DI-water
536 nanofluid in a two-phase closed thermosyphon. *Industrial and Engineering Chemistry Research*,
537 51(3), pp.1423–1428.
- 538 Shanbedi, M. et al., 2012b. Investigation of Heat-Transfer Characterization of EDA-MWCNT / DI-
539 Water Nanofluid in a Two-Phase Closed Thermosyphon. *Industrial & Engineering Chemistry
540 Research*, 51, pp.1423–1428.
- 541 Solomon, A.B. et al., 2013. Thermal performance of anodized two phase closed thermosyphon
542 (TPCT). *Experimental Thermal and Fluid Science*, 48, pp.49–57. Available at:
543 <http://dx.doi.org/10.1016/j.expthermflusci.2013.02.007>.
- 544 Solomon, A.B., Ramachandran, K. & Pillai, B.C., 2012. Thermal performance of a heat pipe with
545 nanoparticles coated wick. *Applied Thermal Engineering*, 36, pp.106–112. Available at:
546 <http://dx.doi.org/10.1016/j.applthermaleng.2011.12.004>.

- 547 Sureshkumar, R., Mohideen, S.T. & Nethaji, N., 2013. Heat transfer characteristics of nanofluids in
548 heat pipes: A review. *Renewable and Sustainable Energy Reviews*, 20, pp.397–410. Available
549 at: <http://dx.doi.org/10.1016/j.rser.2012.11.044>.
- 550 Wang, X. et al., 2012. Effect of Internal Helical Microfin on Condensation Performance of Two-
551 Phase Closed Thermosyphon. *Advanced Materials Research*, 516–517, pp.9–14. Available at:
552 <http://www.scientific.net/AMR.516-517.9>.
- 553 Wong, S.C. & Lin, Y.C., 2011. Effect of copper surface wettability on the evaporation performance:
554 Tests in a flat-plate heat pipe with visualization. *International Journal of Heat and Mass*
555 *Transfer*, 54(17–18), pp.3921–3926. Available at:
556 <http://dx.doi.org/10.1016/j.ijheatmasstransfer.2011.04.033>.
- 557 Yang, X.F., Liu, Z.-H. & Zhao, J., 2008. Heat transfer performance of a horizontal micro-grooved
558 heat pipe using CuO nanofluid. *Journal of Micromechanics and Microengineering*, 18, p.35038.
- 559 Yong, T., Ping, C. & Xiaowu, W., 2010. Experimental investigation into the performance of heat pipe
560 with micro grooves fabricated by Extrusion-ploughing process. *Energy Conversion and*
561 *Management*, 51(10), pp.1849–1854. Available at:
562 <http://dx.doi.org/10.1016/j.enconman.2010.01.001>.

563

- Heat pipe performance is enhanced by making a wall roughness using a new technique.
- A significant reduction in evaporator thermal resistance of 115% is obtained.
- A significant increase in evaporator heat transfer coefficient of 115% is achieved.
- A considerable reduction of 42% in the total thermal resistance is obtained.

ACCEPTED MANUSCRIPT